Journal of Magnetism and Magnetic Materials 321 (2009) 1039–1044

Contents lists available at ScienceDirect

Journal of Magnetism and Magnetic Materials

journal homepage: www.elsevier.com/locate/jmmm

Element-specific spin and orbital moments in $Fe_{1-x}V_x$ alloys

Y. Guan *, C. Scheck, W.E. Bailey

Materials Science Program, Department of Applied Physics, Columbia University, New York 10027, USA

ARTICLE INFO

Article history:
Received 25 May 2008
Received in revised form
2 October 2008
Available online 1 November 2008

PACS:
78.70.Dm
75.50.Bb
75.70.Ak

Keywords:
Transmission-mode XMCD
Fe–V alloy
Sum rule
Orbital-to-spin moment ratio

ABSTRACT

We present transmission-mode X-ray magnetic circular dichroism (XMCD) measurements of element-specific magnetic moments for Fe and V at the $L_{2,3}$ edges in polycrystalline $Fe_{1-x}V_x$ ultrathin films. We find that the orbital-to-spin moment ratio of Fe does not change within experimental error. The V XMCD is not very informative, and a nearly pure-spin type V impurity moment ($\sim$1.0 μ_B/atom, antiparallel to the Fe host moment) is assumed to match known magnetization data. Data are further reduced to a two-sublattice model and found to be compatible with known spectroscopic splitting g-factor data in the alloy. The results confirm that the very low Gilbert damping, attained through the introduction of V into epitaxial $Fe_{1-x}V_x$ films and found by ferromagnetic resonance (FMR), does not result from the reduction of orbital moment content in the alloy.

1. Introduction

The $Fe_{1-x}V_x$ binary alloy system is unique among metallic ferromagnets. Of the three ferromagnetic (FM)–paramagnetic (PM) alloys whose moments adhere to the Slater–Pauling curve [1], only $Fe_{1-x}V_x$ features a strongly polarizable PM constituent. V impurity moments are sizeable, $\sim$1.0 μ_B/atom at small V concentrations, and oriented antiparallel to the Fe host moments by Hund's third rule [2,3]. Cu impurities in Co or Ni possess moments an order of magnitude smaller and parallel to those of the host. Element-specific magnetism in the $Fe_{1-x}V_x$ system has been studied over the years by neutron scattering [2,4–8] and *ab-initio* calculations [3,9–12], with inconsistent results.

Recently, we have found that $Fe_{1-x}V_x$ has the lowest Gilbert damping of any known metallic ferromagnet, to $G = 35$ MHz, 40% lower than that known for pure Fe [13]. Low damping is beneficial for a host of applications in modern spin electronics, from efficient operation in spin momentum transfer (SMT) magnetic random access memory (SMT-MRAM) [14], to proposed novel devices such as the spin torque transistor (STT) [15], to longstanding devices such as integrated, tunable notch filters [16,17]. Questions of element-specific moments in the alloy gain new technological relevance.

Resolution of spin and orbital components of element-specific moments is particularly relevant to understand the low Gilbert damping seen in $Fe_{1-x}V_x$. A longstanding model by Kambersky [18,19] relates the Gilbert relaxation rate G to the balance of spin and orbital moments in the ferromagnet: zero damping is predicted for pure-spin type moments. In $Fe_{1-x}V_x$, the balance of moments begins with a small orbital component ($\sim$10% of total) in Fe; its variation with increasing x in $Fe_{1-x}V_x$ is not well known. While we have addressed this interpretation through (species-averaged) FMR-measured gyromagnetic ratios g_{eff}, finding nearly constant values over the x range of interest [13], the role of the elemental moments of Fe and V in reducing G is still not clear.

X-ray magnetic circular dichroism (XMCD) is an ideally suited technique to answer these questions. Measured in transmission mode, high-quality XMCD spectra can be obtained in the absence of any possible yield saturation effects and field-induced background drift [20,21] which may appear in total-electron-yield (TEY) XMCD data. In Fe, Ni, and Co, element-specific orbital and spin moments can be resolved through dichroism at $L_{2,3}$ edges using sum rules [22,23]. In naturally PM elements, such as V and Cu, the orbital moment sum rule for induced moments is known to hold to good approximation generally; however, the spin moment sum rule is more complicated for light elements, such as V, due to the presence of strong core–hole correlation effects [24,25].

In this article, we present transmission-mode XMCD measurements of Fe and V at the $L_{2,3}$ edges in polycrystalline $Fe_{1-x}V_x$

* Corresponding author. Tel.: +1 914 945 1772.
E-mail address: yguan@us.ibm.com (Y. Guan).

0304-8853/$ - see front matter © 2008 Elsevier B.V. All rights reserved.
doi:10.1016/j.jmmm.2008.10.014

(5 nm) samples over the range of $0 \leqslant x \leqslant 0.15$. Using sum rules, we find a linear reduction of Fe moment as a function of increasing V concentration, with the rate of $\sim 0.012\,\mu_B$ per%V ($\sim 1.2\,\mu_B$ per V atom). The reduction is compared with previously reported neutron scattering measurements [2,4–8] and *ab-initio* calculations [9–12]. In addition, we find that orbital-to-spin moment ratios for Fe are mostly unchanged over the measured range. The V XMCD is not very informative, and we assume a nearly pure-spin type V impurity moment ($\sim 1.0\,\mu_B$/atom, antiparallel to the Fe host moment) to match known magnetization behavior. An overall picture for element-specific spin and orbital moments of Fe and V in the alloy is discussed with respect to known magnetization and g_{eff} data.

2. Experiment

Polycrystalline alloys of $Fe_{1-x}V_x$ (5 nm) ultrathin films were deposited onto commercially available, supported semitransparent Si_3Ni_4 membrane windows (1.0 mm square and 75 nm thick), by using UHV magnetron cosputtering from elemental Fe and V targets at a base pressure of 4×10^{-9} Torr.

V-doped ultrathin Fe films (5 nm thick), with doping levels of 0%, 5%, and 15%, were investigated in the study. All these films were grown with a 5 nm Ti seed and a 2 nm Ti cap layer to improve growth and prevent oxidation, respectively. Atomic fluxes of each sputtering source to the substrate, operating separately, were calibrated using a quartz crystal monitor, located in front of the substrate position, immediately prior to film deposition. Rates for each alloy composition were subsequently calibrated using the atomic force microscopy (AFM).

$L_{2,3}$-edge XMCD spectra of Fe and V were measured in transmission mode at the UV ring of the National Synchrotron Light Source (NSLS), Brookhaven National Laboratory, soft X-ray Beamline U4B. XMCD was measured for fixed circular photon helicity, 70% polarization, with pulsed magnetization switching ($H = \pm 280$ Oe) at the sample; photon incidence was fixed at 45° with respect to the sample normal. The samples were mounted with magnetic easy axis almost along the applied field direction. Measurements were taken at remanence (held at zero field), where the transmitted intensity was read at a soft X-ray sensitive photodiode and normalized to an incident intensity at a reference grid. In order to correct for any drift in the monochromator which may lead to derivative-like artifacts in XMCD, XMCD measurements with $H+$ ($M+$) measured first and $H-$ ($M-$) measured second were averaged with measurements taken in reversed order ("duplex mode") [21]. The MCD data were divided by the factor of $0.70 \cos 45^\circ$ to correct for non-grazing incidence and incomplete circular polarization. Background spectra $I_S(\omega)$ from the bare Si_3N_4 (membrane)/Ti(7 nm) were recorded for each energy interval and applied in the background subtraction. All XMCD measurements were carried out at room temperature.

Fe XMCD hysteresis loops were taken by setting the photon energy to the L_3 peak of Fe at 707.2 eV. The ratio of remanence-to-saturation field (M_r/M_s) will be estimated and used to obtain a calibration factor for the calculation of Fe orbital and spin moments.

3. Results and discussion

Fig. 1 shows Fe XMCD hysteresis loops for $Fe_{1-x}V_x$ ultrathin films. The ratios of remanence-to-saturation field (M_r/M_s) are estimated to be 0.65 for pure Fe, 0.92 for $Fe_{0.95}V_{0.05}$, and 0.73 for $Fe_{0.85}V_{0.15}$. The remanent fraction has an estimated error of ~5%. XMCD spectra were taken in remanence, so these ratios will be used as calibration factors for calculation of Fe orbital and spin moments by means of sum rules.

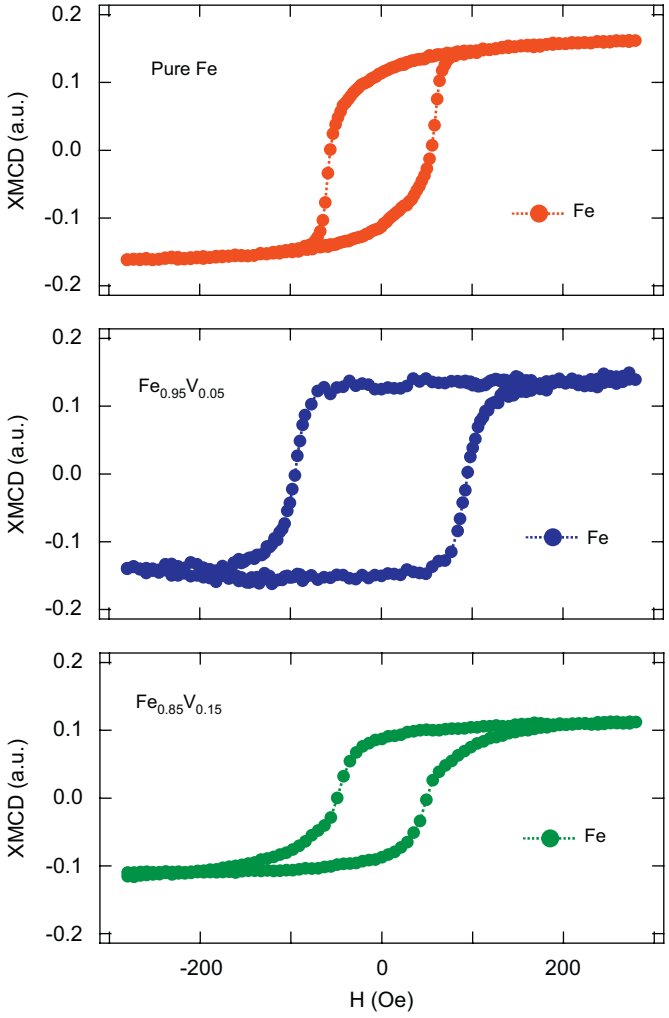

Fig. 1. (Color online) Fe XMCD hysteresis loops for pure Fe (top), $Fe_{0.95}V_{0.05}$ (middle) and $Fe_{0.85}V_{0.15}$ (bottom) ultrathin films.

According to sum rules [22,23], the magnitude of elemental moments is proportional to the magnetic circular dichroism (MCD, difference in absorption on magnetization switching) normalized to the X-ray absorption (XAS, averaged for magnetization switching). Spin-to-orbital moment ratios are given by the relative weight of MCD at the L_3 edge (p) to that at the L_2 edge (q); r denotes summed XAS above background. At the $L_{2,3}$ edges of transition metals (e.g., Fe), orbital and spin moments are given by (neglecting the $\langle \hat{T}_z \rangle / \langle \hat{S}_z \rangle$ term, $c = 1, l = 2$ [23])

$$m_{orb} = \frac{-4q(10 - n_{3d})}{3r} \times \frac{M_s}{M_r}, \tag{1}$$

$$m_{spin} = \frac{-(6p - 4q)(10 - n_{3d})}{r} \times \frac{M_s}{M_r}, \tag{2}$$

where n_{3d} is the 3d electron occupation number of the specific transition metal atom. M_r/M_s is the calibration factor due to the in-remanence detection mode, obtained from the Fe XMCD hysteresis loops (see Fig. 1). Detailed data analysis needed for the application of the sum rules to the transmission-mode XMCD spectra can follow the established procedure of Chen et al. [20] and our previous work [21].

Fig. 2 shows the $L_{2,3}$-edge MCD and summed XAS spectra of V and their integrations calculated from the spectra for the

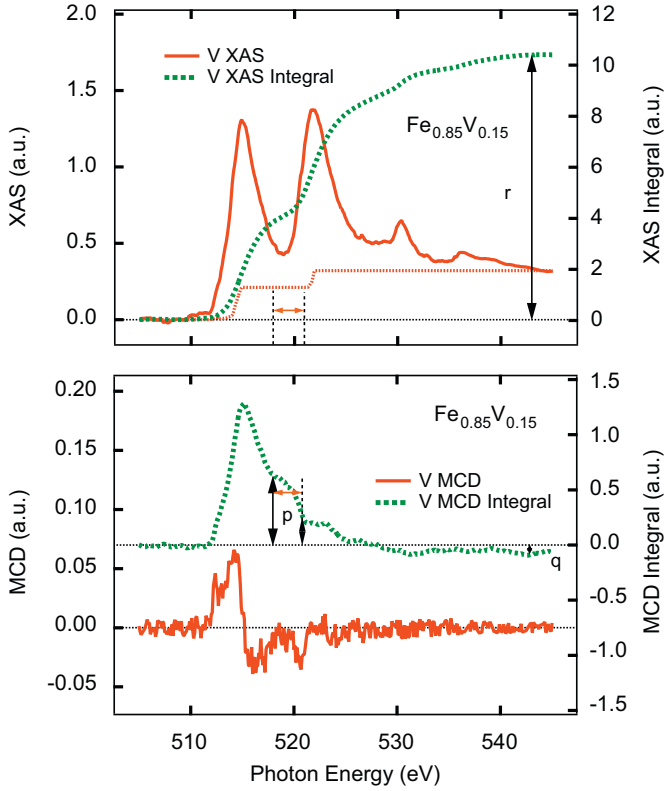

Fig. 2. (Color online) $L_{2,3}$-edge transmission XAS and MCD spectra of V in $Fe_{0.85}V_{0.15}$ ultrathin film: summed XAS spectra and its integral (top); MCD spectra and its integral (bottom). The ambiguity of the p position are due to the presence of a small spin–orbit splitting (~6.8 eV) and a strong electron core–hole interaction.

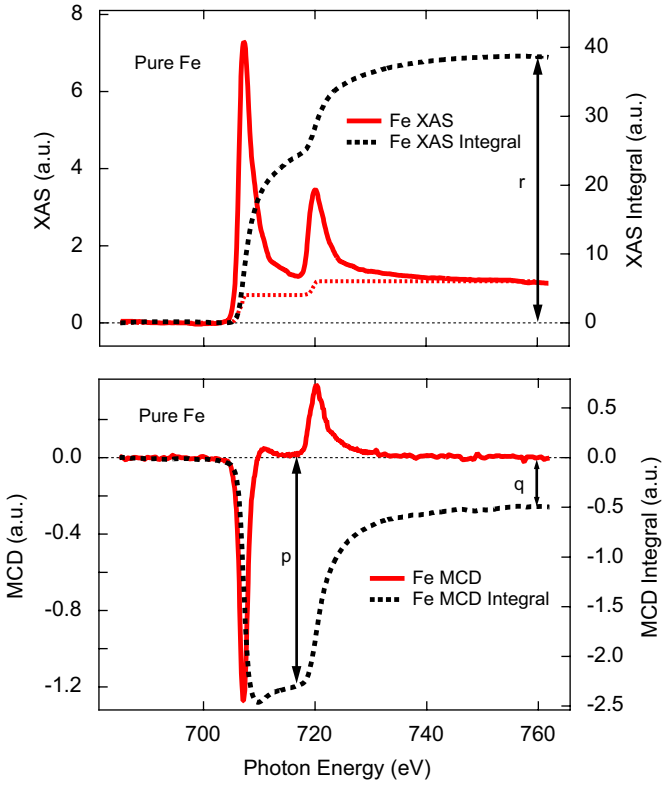

Fig. 3. (Color online) $L_{2,3}$-edge transmission XAS and MCD spectra of Fe in pure Fe ultrathin film: summed XAS spectra and its integral (top); MCD spectra and its integral (bottom).

$Fe_{0.85}V_{0.15}$ ultrathin film. The branching ratio of the summed XAS spectrum of V is close to 1:1 due to the presence of a strong electron core–hole interaction [24], similar to that of the previously reported XAS spectra of V in the disordered $Fe_{0.90}V_{0.10}$ alloy measured by TEY-mode XMCD [26]. The $L_{2,3}$ edges of the summed V XAS spectrum partially overlap due to the small spin–orbit splitting (~6.8 eV) of the core states, which also leads to a complicated shape of the V dichroism. The presence of two additional non-V absorption peaks above 530 eV in the summed V XAS spectrum may arise from the K edge absorption of oxygen. For the V MCD spectrum, the noisy V dichroism is probably due to the low V concentration in the sample. Contrary to the Fe dichroism in the same sample shown in Fig. 5, the V dichroism reveals a positive onset at the L_3 edge and a negative intensity at the L_2 edge, which indicates an antiparallel alignment between Fe host moment and induced V impurity moment, in agreement with previous experiments [2,26,27].

Assuming a value of $n_{3d} = 3.56$ for V [26], we apply sum rules [22,23] to the V XMCD spectra to determine the projected orbital (m^V_{orb}) and spin (m^V_{spin}) moment values for V element. We find the induced V impurity moment in the $Fe_{0.85}V_{0.15}$ ultrathin film is composed of an orbital part of $0.06 \pm 0.03\,\mu_B$/atom and an antiparallel aligned spin part of $2.5 \pm 2\,\mu_B$/atom, with the experimental uncertainty estimated by taking p, q, and r integrals over slightly different portions of the pre-edge and post-edge regions. The significant experimental error bars of the application of sum rules to the V XMCD spectra come primarily from the ambiguity of the p position, due to the presence of a small spin–orbit splitting (~6.8 eV) and a strong electron core–hole interaction which leads to apparent overlap of the $L_{2,3}$ edges [24]. In addition, the noise in the V dichroism and the additional non-V features in the summed V XAS spectrum will probably introduce some small artificial magnetic background signals in the V XMCD spectra and further reduce the reliability of the results of the sum rules analysis. The observed V impurity moment (m^V, calculated by Eq. (5)) is larger than the value of $-0.18\,\mu_B$/atom determined by TEY-mode XMCD for a disordered $Fe_{0.90}V_{0.10}$ alloy [26]. The error bar of m^V only catches the edge of the value of $-0.82\,\mu_B$/atom determined by polarized neutron diffuse scattering for a polycrystalline $Fe_{1-x}V_x$ sample with $x = 0.15$ [2]. We believe that the discrepancy illustrates the difficulties in applying the spin sum rule for $L_{2,3}$ edges of early 3d elements [24,25,28].

Figs. 3–5 shows the $L_{2,3}$-edge MCD and summed XAS spectra of Fe and their integrations calculated from the spectra for each of the $Fe_{1-x}V_x$ samples. Assuming a value of $n_{3d} = 6.6$ for Fe [20,29], we apply sum rules [22,23] to the Fe XMCD spectra to determine the projected orbital to spin moment ratios ($m^{Fe}_{orb}/m^{Fe}_{spin}$), as well as the individual projected orbital (m^{Fe}_{orb}) and spin (m^{Fe}_{spin}) moment values for Fe element. Results are listed in Table 1, where the experimental error bars are estimated to be 5% for $m^{Fe}_{orb}/m^{Fe}_{spin}$ and 10% for m^{Fe}_{orb} and m^{Fe}_{spin}.

As shown in Table 1, the total projected Fe moment (m^{Fe}, calculated by Eq. (4)) estimates are found to be $1.69\,\mu_B$/atom for pure Fe, $1.63\,\mu_B$/atom for $Fe_{0.95}V_{0.05}$, and $1.51\,\mu_B$/atom for $Fe_{0.85}V_{0.15}$. The observed Fe moment value for 5 nm pure Fe is smaller by $\sim 0.5\,\mu_B$/atom than the reported value of $\sim 2.2\,\mu_B$/atom for bulk Fe [1]. We attribute this to reduced Fe moments due to intermixing in the Ti seed and cap layer [29]. In addition, we assume similar moment reduction effects from Ti intermixing in all the $Fe_{1-x}V_x$ alloys.

The estimates of Fe moment assume a constant number of d-holes ($10 - n_{3d}$) for Fe in the $Fe_{1-x}V_x$ alloy series. Using this assumption, we find a linear decrease of Fe moments with increasing V concentration over the measured range of

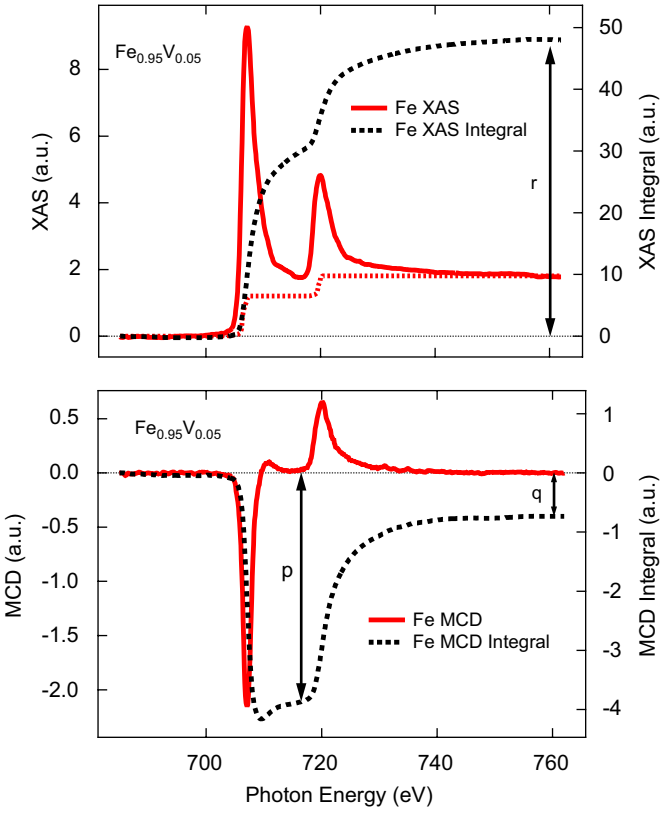

Fig. 4. (Color online) $L_{2,3}$-edge transmission XAS and MCD spectra of Fe in $Fe_{0.95}V_{0.05}$ ultrathin film: summed XAS spectra and its integral (top); MCD spectra and its integral (bottom).

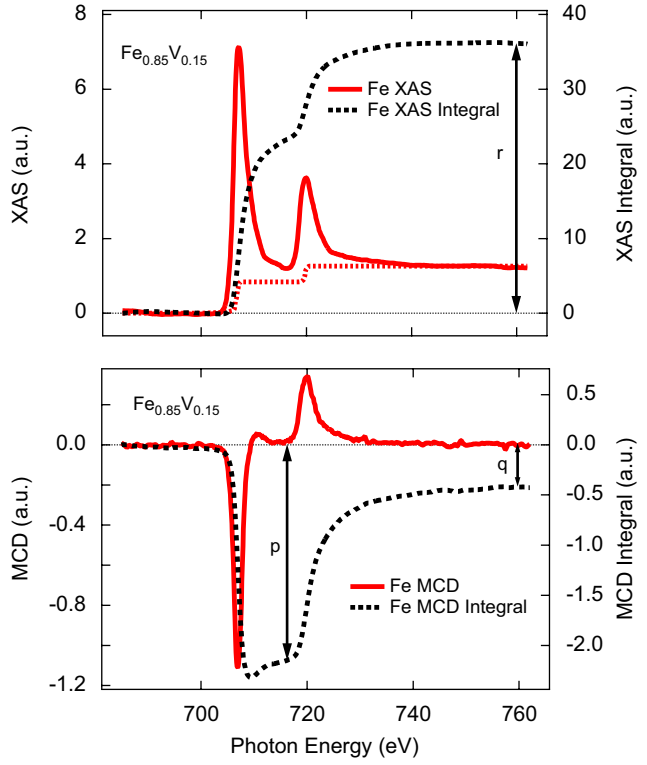

Fig. 5. (Color online) $L_{2,3}$-edge transmission XAS and MCD spectra of Fe in $Fe_{0.85}V_{0.15}$ ultrathin film: summed XAS spectra and its integral (top); MCD spectra and its integral (bottom).

Table 1
Projected orbital (m^{Fe}_{orb}) and spin (m^{Fe}_{spin}) magnetic moments of Fe element in pure Fe, $Fe_{0.95}V_{0.05}$, and $Fe_{0.85}V_{0.15}$ ultrathin films, as well as orbital to spin moment ratios ($m^{Fe}_{orb}/m^{Fe}_{spin}$) and total projected Fe moment of $m_{Fe} = m^{Fe}_{orb} + m^{Fe}_{spin}$.

	Pure Fe	$Fe_{0.95}V_{0.05}$	$Fe_{0.85}V_{0.15}$
$m^{Fe}_{orb}/m^{Fe}_{spin}$	0.055	0.049	0.051
m^{Fe}_{orb} (μ_B/atom)	0.088	0.076	0.073
m^{Fe}_{spin} (μ_B/atom)	1.60	1.55	1.44
m^{Fe} (μ_B/atom)	1.69	1.63	1.51

The experimental error bars are estimated to be 5% for $m^{Fe}_{orb}/m^{Fe}_{spin}$ and 10% for m^{Fe}_{orb} and m^{Fe}_{spin}.

$0 \leqslant x \leqslant 0.15$, with the rate of $\sim 0.012\,\mu_B$ per %V ($\sim 1.2\,\mu_B$ per V atom).

In Table 2, we list composition-dependent estimates of Fe moment change (Δm^{Fe}), V impurity moment (m^V) and total moment change (Δm^{total}) in $Fe_{1-x}V_x$ alloys for V composition up to 30%. Data are taken from our transmission-mode XMCD measurements and collected from the literature, including experimental and theoretical values from the various techniques [2,4–12,26]. The total moment (m^{total}) estimates of $Fe_{1-x}V_x$ can be calculated by the following equations:

$$m^{total} = (1-x) \times m^{Fe} + x \times m^{V}, \tag{3}$$

$$m^{Fe} = m^{Fe}_{orb} + m^{Fe}_{spin}, \tag{4}$$

$$m^{V} = m^{V}_{orb} - m^{V}_{spin}, \tag{5}$$

where the relative alignment of the orbital and spin moment of Fe and V obeys Hund's third rule. The negative sign of m^V that appeared in Table 2 indicates an antiparallel alignment between Fe and V moments. As shown in Table 2, the estimated reduction in Fe moments ($\sim 1.2\,\mu_B$ per V atom) from our transmission-mode XMCD is on the highest end of the range predicted by *ab-initio* calculations [9,10,12] and reported in previous neutron scattering measurements [2,4–8].

Including the compositional dependence of Fe moment into Eq. (3) and ignoring the second-order term, the total moment of $Fe_{1-x}V_x$ alloy can be approximated by

$$m^{total} \approx m^{Fe}_0 - [m^{Fe}_0 - \Delta m^{Fe} - m^{V}] \times x, \tag{6}$$

where m^{Fe}_0 denotes Fe moment value for pure Fe. Assuming $m^{Fe}_0 \approx 2.23\,\mu_B$/atom in Eq. (6), the estimated Fe moment reduction of $\sim 1.2\,\mu_B$ per V atom would seem to imply that $m^V \approx +0.14\,\mu_B$/atom, when reconciled with previously reported magnetization data of $m^{total} \approx (2.23 - 3.29 \times x)\,\mu_B$/atom for $Fe_{1-x}V_x$ alloys [30]. This value of m^V is inconsistent with Hund's third rule, which predicts V impurity moments to be oriented antiparallel to the Fe host moments. As discussed before, the V XMCD was not very informative, where significant experimental error bars exist due to the difficulties in applying spin sum rules to the V XMCD spectra. Therefore, if instead one assumes an estimated V impurity moment value of $-1.0\,\mu_B$/atom [2,3] in Eq. (6), only a small Fe moment reduction of $\sim 0.06\,\mu_B$ per V atom would be needed in order to match previously reported magnetization data for $Fe_{1-x}V_x$ alloys [30]. We regard the latter interpretation as more sensible due to the absence of data for compositional-dependent d-hole numbers of Fe in the alloy.

It is well known that the orbital-to-spin moment ratio (m_{orb}/m_{spin}) is more easily derived from XMCD. Using sum rules, we have determined the $m^{Fe}_{orb}/m^{Fe}_{spin}$ estimates as 0.055 for pure Fe, 0.049 for $Fe_{0.95}V_{0.05}$, and 0.051 for $Fe_{0.85}V_{0.15}$ (shown in Table 1). These values agree within a constant value of 0.049 ± 0.005. In a two-sublattice model [10,31,32], the species-averaged

Table 2
Compositional dependence of Fe moment change (Δm^{Fe}), V impurity moment (m^{V}) and total moment change (Δm^{total}) in $Fe_{1-x}V_x$ alloys.

Technique	x	$\Delta m^{Fe}(\mu_B/\text{atom V})$	$m^{V}(\mu_B/\text{atom})$	$\Delta m^{total}(\mu_B/\text{atom V})$
Neutron diffraction [4–6]	Dilute limit	−0.10	−0.90	
Unpolarized neutron scattering [7,8]	0.06	-0.3 ± 0.6	-0.56 ± 0.07	-2.76 ± 0.04
	0.10	-0.4 ± 0.3	-0.66 ± 0.06	-2.84 ± 0.03
	0.15	-1.1 ± 0.2	-0.10 ± 0.06	-2.16 ± 0.03
	0.21	-1.5 ± 0.2	0.15 ± 0.07	-1.75 ± 0.04
Polarized neutron scattering [2]	0.06	0.4 ± 0.4	-1.11 ± 0.05	-3.35 ± 0.03
	0.10	0.1 ± 0.3	-1.07 ± 0.06	-3.30 ± 0.03
	0.15	-0.2 ± 0.3	-0.82 ± 0.08	-3.00 ± 0.06
	0.21	-0.4 ± 0.2	-0.76 ± 0.06	-2.89 ± 0.03
TEY-mode XMCD [26]	0.10		−0.18	
Transmission-mode XMCD	0.05	−1.2		
	0.15	−1.2	-2.4 ± 2	
CPA calculations [9]	Fe-rich region	−0.18		
Green-function method [10]	Fe-rich region	−0.21	−1.71	
	0.10	−0.40	−1.07	−3.70
	0.20	−0.95	−0.40	−3.40
	0.30	−1.5	−0.27	−3.57
Lloyd's formula [11]	Dilute limit		−0.96	−3.37
First-principles DV method [12]	Fe-rich region	−0.36	−0.86	

Data are taken from our transmission-mode XMCD measurements and collected from the literature, including experimental and theoretical values from the various techniques.

orbital-to-spin moment ratios (m_{orb}/m_{spin}) for the entire $Fe_{1-x}V_x$ films can be obtained by

$$\frac{m_{orb}}{m_{spin}} \cong \frac{(1-x)\times m_{orb}^{Fe} + x \times m_{orb}^{V}}{(1-x)\times m_{spin}^{Fe} - x \times m_{spin}^{V}}, \quad (7)$$

where the orbital moments of Fe and V are oriented parallel but the spin moments are aligned antiparallel, confirmed by the orbital sum rules and the opposite sign of L_3 onsets for Fe and V XMCD spectra in the sample. Furthermore, the orbital-to-spin moment ratios (m_{orb}/m_{spin}) can be related to the spectroscopic splitting g-factor (g_{eff}) by [33–35]

$$g_{eff} \cong 2 \times \left(1 + \frac{m_{orb}}{m_{spin}}\right). \quad (8)$$

Based on Eqs. (7) and (8), using the previously reported magnetization data for $Fe_{1-x}V_x$ alloys [30], the observed orbital-to-spin moment ratio of 0.049 ± 0.005 for Fe, and assuming $m_0^{Fe} \approx 2.23\,\mu_B$/atom and zero orbital moment (pure spin) on V sites, the estimates of g_{eff} for the entire $Fe_{1-x}V_x$ films can be approximated by

$$g_{eff} \approx 2 \times \left[1 + \frac{0.10 \times (1-x)}{(2.23 - 3.29 \times x) - 0.10 \times (1-x)}\right]. \quad (9)$$

Based on Eq. (9), the estimates of g_{eff} are calculated up to $x = 0.55$ and plotted in Fig. 6 as a function of V doping concentration x. The previous reported g_{eff} values for the entire epitaxial $Fe_{1-x}V_x$ films (8 and 50 nm, respectively) by FMR [13] are also included for comparison. As shown in Fig. 6, g_{eff} increases very slowly with increasing V doping concentration x over the small concentrations of $0 \leqslant x \leqslant 0.20$ but increases more rapidly at higher concentrations up to $x = 0.55$, in reasonable agreement with those found by FMR [13] within experimental error. This increasing trend in the change of g_{eff} as a function of x confirms that the very low Gilbert damping found in epitaxial $Fe_{1-x}V_x$ films by FMR [13] is not attributable to orbital moment reduction in the alloy.

We summarize the picture of the Fe–V system which emerges from our transmission-mode XMCD measurements. We find nearly constant m_{orb}/m_{spin} values on Fe (~0.049, over the measured range of $0 \leqslant x \leqslant 0.15$ in the $Fe_{1-x}V_x$ alloys). The V XMCD is not very informative, and a nearly pure-spin type V impurity moment (~1.0 μ_B/atom, antiparallel to the Fe host moment) is assumed to match known magnetization behavior. This picture is consistent with g_{eff} data within a two-sublattice model; we do not rely on the XMCD-derived value for the induced V impurity moment in this picture. The total Fe moment analysis from XMCD, however, yields a linear reduction of Fe moment with V addition (by ~1.2 μ_B per V atom) which is unphysical; we regard it as an artifact resulting from the assumption of constant n_{3d} for Fe in the $Fe_{1-x}V_x$ alloy series. The results confirm that the very low Gilbert damping found in epitaxial $Fe_{1-x}V_x$ films by FMR does not result from the reduction of orbital moment content in the alloy.

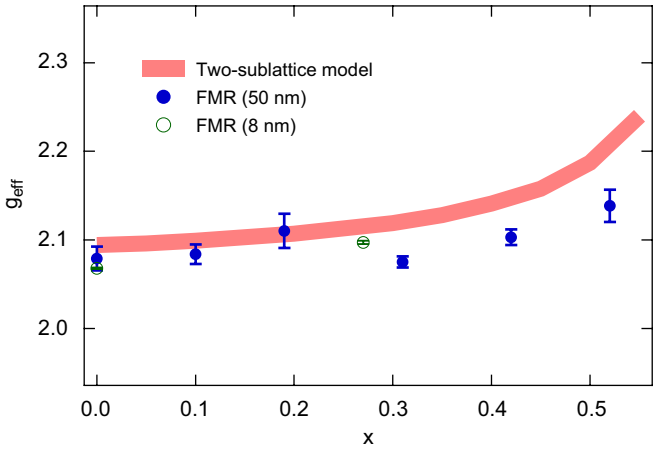

Fig. 6. (Color online) Compositional dependence of spectroscopic splitting g-factor (g_{eff}) for the entire $Fe_{1-x}V_x$ (5 nm) ultrathin films determined in a two-sublattice model. Previously reported g-factor values for the entire epitaxial $Fe_{1-x}V_x$ films (8 and 50 nm, respectively) by FMR [13] are included for comparison.

4. Conclusion

We have performed transmission-mode XMCD measurements in polycrystalline $Fe_{1-x}V_x$ ultrathin films over the range of $0 \leqslant x \leqslant 0.15$. Element-specific orbital, spin, and total magnetic moments have been estimated for Fe and V using sum rules analysis. Salient results are nearly constant m_{orb}/m_{spin} values on Fe (~0.049, over the measured range of $0 \leqslant x \leqslant 0.15$ in the $Fe_{1-x}V_x$ alloys). The V XMCD is not very informative, and nearly pure-spin type V impurity moment (~1.0 μ_B/atom, antiparallel to the Fe

host moment) is assumed to match known magnetization behavior. Data are found to be compatible with spectroscopic splitting g-factor data in the alloy within a two-sublattice model. The results confirm that the very low Gilbert damping found in epitaxial $Fe_{1-x}V_x$ films by FMR is not attributable to orbital moment reduction in the alloy.

Acknowledgments

The authors thank Dario A. Arena for beamline support. This work was partially supported by the National Science Foundation with Grant no. NSF-DMR-02-39724, and has used the shared experimental facilities that are supported primarily by the MRSEC (Columbia) program of the National Science Foundation under no. NSF-DMR-0213574. Research was carried out in part at the National Synchrotron Light Source, Brookhaven National Laboratory, which is supported by the US Department of Energy, Division of Materials Sciences and Division of Chemical Sciences, under Contract no. DE-AC02-98CH10886.

References

[1] R.C. O'Handley, Modern Magnetic Materials: Principles and Applications, Wiley, New York, 2000.
[2] I. Mirebeau, G. Parette, J.W. Cable, J. Phys. F Met. Phys. 17 (1987) 191.
[3] D.D. Johnson, F.J. Pinski, J.B. Staunton, J. Appl. Phys. 61 (1987) 3175.
[4] G.G. Low, M.F. Collins, J. Appl. Phys. 34 (1963) 1195.
[5] M.F. Collins, G.G. Low, Proc. Phys. Soc. 86 (1965) 535.
[6] I.A. Campbell, Proc. Phys. Soc. 89 (1966) 71.
[7] I. Mirebeau, G. Parette, J. Appl. Phys. 53 (1982) 1960.
[8] I. Mirebeau, M.C. Cadeville, G. Parette, I.A. Campbell, J. Phys. F Met. Phys. 12 (1982) 25.
[9] N. Hamada, H. Miwa, Prog. Theor. Phys. 59 (1978) 1045.
[10] A.Z. Maksymowicz, Physica B 149 (1988) 240.
[11] B. Drittler, N. Stefanou, S. Blügel, R. Zeller, P.H. Dederichs, Phys. Rev. B 40 (1989) 8203.
[12] J.C. Krause, C. Paduani, J. Schaff, M.I. da Costa Jr., Phys. Rev. B 57 (1998) 857.
[13] C. Scheck, L. Cheng, I. Barsukov, Z. Frait, W.E. Bailey, Phys. Rev. Lett. 98 (2007) 117601.
[14] J. Slonczewski, J. Magn. Magn. Mater. 195 (1999) 261.
[15] G.E.W. Bauer, A. Brataas, Y. Tserkovnyak, B.J. Van Wees, Appl. Phys. Lett. 82 (2003) 3928.
[16] N. Smith, P. Arnett, Appl. Phys. Lett. 78 (2001) 1448.
[17] C. Scheck, L. Cheng, W.E. Bailey, Appl. Phys. Lett. 88 (2006) 252510.
[18] V. Kamberský, Can. J. Phys. 48 (1970) 2906.
[19] J. Kuneš, V. Kamberský, Phys. Rev. B 65 (2002) 212411.
[20] C. Chen, Y.U. Idzerda, H.-J. Lin, N.V. Smith, G. Meigs, E. Chaban, G.H. Ho, E. Pellegrin, F. Sette, Phys. Rev. Lett. 75 (1995) 152.
[21] Y. Guan, Z. Dios, D.A. Arena, L. Cheng, W.E. Bailey, J. Appl. Phys. 97 (2005) 10A719.
[22] B. Thole, P. Carra, F. Sette, G. van der Laan, Phys. Rev. Lett. 68 (1992) 1943.
[23] P. Carra, B. Thole, M. Altarelli, X. Wang, Phys. Rev. Lett. 70 (1993) 694.
[24] J. Schwitalla, H. Ebert, Phys. Rev. Lett. 80 (1998) 4586.
[25] E. Goering, Philos. Mag. 85 (2005) 2895.
[26] A. Scherz, H. Wende, K. Baberschke, J. Minár, D. Benea, H. Ebert, Phys. Rev. B 66 (2002) 184401.
[27] M.M. Schwickert, R. Coehoorn, M.A. Tomaz, E. Mayo, D. Lederman, W.L. O'Brien, T. Lin, G.R. Harp, Phys. Rev. B 57 (1998) 13681.
[28] A. Scherz, H. Wende, C. Sorg, K. Baberschke, J. Minár, D. Benea, H. Ebert, Phys. Scr. T 115 (2005) 586.
[29] A. Scherz, H. Wende, P. Poulopoulos, J. Lindner, K. Baberschke, P. Blomquist, R. Wäppling, F. Wilhelm, N.B. Brooks, Phys. Rev. B 64 (2001) 180407(R).
[30] M.V. Nevitt, A.T. Aldred, J. Appl. Phys. 34 (1963) 463.
[31] M. Plischke, D. Mattis, Phys. Rev. B 7 (1973) 2430.
[32] A.Z. Maksymowicz, J. Phys. F 12 (1982) 537.
[33] C. Kittel, Phys. Rev. 76 (1949) 743.
[34] J.H. Van Vleck, Phys. Rev. 78 (1950) 266.
[35] A.J.P. Meyer, G. Asch, J. Appl. Phys. 32 (1961) 330S.